Graphene-supported 2D cobalt oxides for catalytic applications

Loïc Michel, Sécou Sall, Thierry Dintzer, Cerise Robert, Antoine Demange, Valérie Caps

Faraday Discussions

Accepted Manuscript

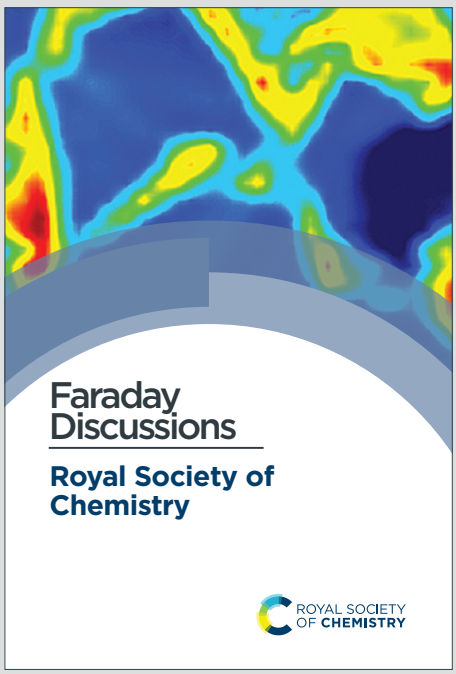

This article can be cited before page numbers have been issued, to do this please use: L. Michel, S. Sall, T. Dintzer, C. Robert, A. Demange and V. Caps, *Faraday Discuss.*, 2019, DOI: 10.1039/C9FD00110G.

ROYAL SOCIETY OF CHEMISTRY

www.rsc.org/faraday_d

View Article Online
DOI: 10.1039/C9FD00110G

ARTICLE

Graphene-supported 2D cobalt oxides for catalytic applications

Loïc Michel,[a] Sécou Sall, [a] Thierry Dintzer, [a] Cerise Robert, [a] Antoine Demange [a] and Valérie Caps [a] *

Received 00th January 20xx,
Accepted 00th January 20xx

DOI: 10.1039/x0xx00000x

2D materials are attracting increasing attention in many strategic applications. In particular, ultra-thin non-layered oxides have been shown to outperform their 3D counter-parts in several health and energy applications, such as the removal of toxic carbon monoxide by low temperature oxidation and the development of high performance supercapacitors. The general reason for that is the increased surface-to-volume ratio, which allows to maximize exposure of active species and enhance exchange between the (limited) bulk and the surface. The challenge is to synthesize such 2D configurations of 3D oxides, which generally requires quite harsh multi-step, multi-reagent chemical processes. Here we show that natural graphite can be used as a templating matrix to grow non-stoichimetric 2D transition metal oxides. We focus on highly porous, highly reduced cobalt oxides grown from cobalt nitrate and sodium borohydride under sonication. Extensive characterization, including nitrogen physisorption, thermogravimetric analysis (TGA), scanning and transmission electron microscopies (SEM/TEM), X-ray diffraction (XRD), temperature programmed oxidation and reduction (TPO/TPR), Fourier Transformed Infrared (FTIR) and Raman spectroscopies, highlights the specific features of the 2D morphologies (nanosheets and nanofilms) obtained. For comparison, 3D morphologies of Co_3O_4 spinel nanocrystallites are grown from stacked 2D cobalt phthalocyanine-graphene precursors upon controlled thermal oxidation. Finally, low temperature CO oxidation catalysis evidences the superior performance of the graphene-supported CoO-like cobalt oxide 2D nanosheets.

Introduction

2D materials have attracted increasing attention for energy applications in the last years. There are numerous examples of 2D materials outperforming their 3D counter-parts in the catalysis,[1, 2] electrocatalysis[3] and photocatalysis[4] fields. In particular, ultra-thin non-layered oxides have proven more efficient than their 3D counter-parts, for e.g. low temperature oxidation catalysis, supercapacitors,[5] water splitting[4] or CO_2 photoreduction.[6] The general reason for that is the high number of defects, namely oxygen vacancies, achievable by these strained configurations.[3,7] Number of adsorption and active sites and oxygen mobility are thus increased. The challenge is to stabilize such 2D configurations of 3D oxides. Nanosheets of cobalt oxides for example are synthesized essentially by controlled hydrothermal/solvothermal methods, in the presence of surfactants, such as urea,[8] ethylene glycol,[9] PVP [10] and coordination polymers,[11] amongst others. Top down methods, such as oxidation-assisted dealloying in highly alkaline solutions, can also be used.[12] In all these methods, quite stringent reaction conditions, prolonged reaction times, elevated temperatures and/or complex reaction mixtures are required. We have been using hard templating techniques for the synthesis of 3D arrays of 1D carbon nanorods.[13, 14] More recently, we used agglomerated titania nanoparticles as a 3D templating matrix to grow 2D graphitic carbon nitride with limited thickness and promising photocatalytic activity for solar H_2 production from water.[15]

Here we show that natural graphite can be used as a templating matrix to grow non-stoichiometric 2D transition metal oxides under mild conditions. We focus on highly reduced 2D cobalt oxides with high specific surface areas (up to 180 m^2/g). We describe the sonication-assisted bottom-up chemical synthesis methodology used and the impact of some relevant parameters, including the metal precursor, on the oxide texture and reducibility, as probed by N_2 physisorption, TGA, SEM, TEM, XRD, TPO/TPR, FTIR and Raman spectroscopies. The resulting graphene-supported cobalt oxides exhibit remarkably low temperature activity for CO oxidation catalysis, which will be discussed in light of their compositional and structural features.

Results and discussion

Synthesis of graphene-supported cobalt oxides.

General methodology. The materials were synthesized in one pot from bulk graphite and a cobalt precursor, using conditions inspired from those used for the sonication-assisted exfoliation of graphite in the liquid phase.[16] In this study, we have used dimethylformamide (DMF) as solvent and "soft" exfoliating agent. The presence of the cobalt precursor during the exfoliating process is designed to allow intercalation of the metal compound between graphene layers and possible metal deposition on top of graphene layers, depending on the affinity between the cobalt compound and

[a] Institut de Chimie et des Procédés pour l'Energie, l'Environnement et la Santé (ICPEES), CNRS UMR 7515 / University of Strasbourg, 25 rue Becquerel, 67087 Strasbourg, France.
* Corresponding author. E-mail: caps@unistra.fr
Electronic Supplementary Information (ESI) available: [details of any supplementary information available should be included here]. See DOI: 10.1039/x0xx00000x

the extended π network of the graphene surface. Two types of cobalt precursors have been used: a cobalt complex known to π-stack with graphene-type surfaces, namely cobalt phthalocyanine (CoPc), and a cobalt salt (cobalt nitrate, CoNO3) in combination with sodium borohydride ($NaBH_4$) to induce chemical reduction of Co^{2+}.[17,18]

Exfoliation state of graphite in the composites. After limited reaction time, typically 15 min, under sonication, the dried composites are found to contain about 5 and 7% Co, for CoPc/graphene and CoNO3/graphene, respectively, based on ICP-OES measurements. In both composites, the XRD reflection relative to the C(002) stacking order of graphite at 2θ = 26.5° is much weaker than in the parent graphite (Figure 1 a). This shows that graphite has been exfoliated in the metal incorporation process. It is also much weaker than in the material resulting from graphite sonication in DMF only (absence of metal compounds). This further suggests that incorporated metal compounds are intercalated and trapped in-between graphene layers, acting as permanent exfoliating agent and preventing long-range stacking of graphene planes.[19] Smaller stacks of graphene layers are thus stabilized by the presence of the metal compounds in the dried composites.

CoPc-derived composites. For CoPc/graphene, FTIR (Figure 1 b) and Raman (Figure 1 c) spectra clearly show the presence of the full CoPc complex in the dried composite. Comparison of the FTIR spectra of the composite and the free CoPc complex however reveals that the out-of-plane N-H vibrations are much weaker (relative to the in-plane aromatic C-C and C-N vibrations) in the composite.

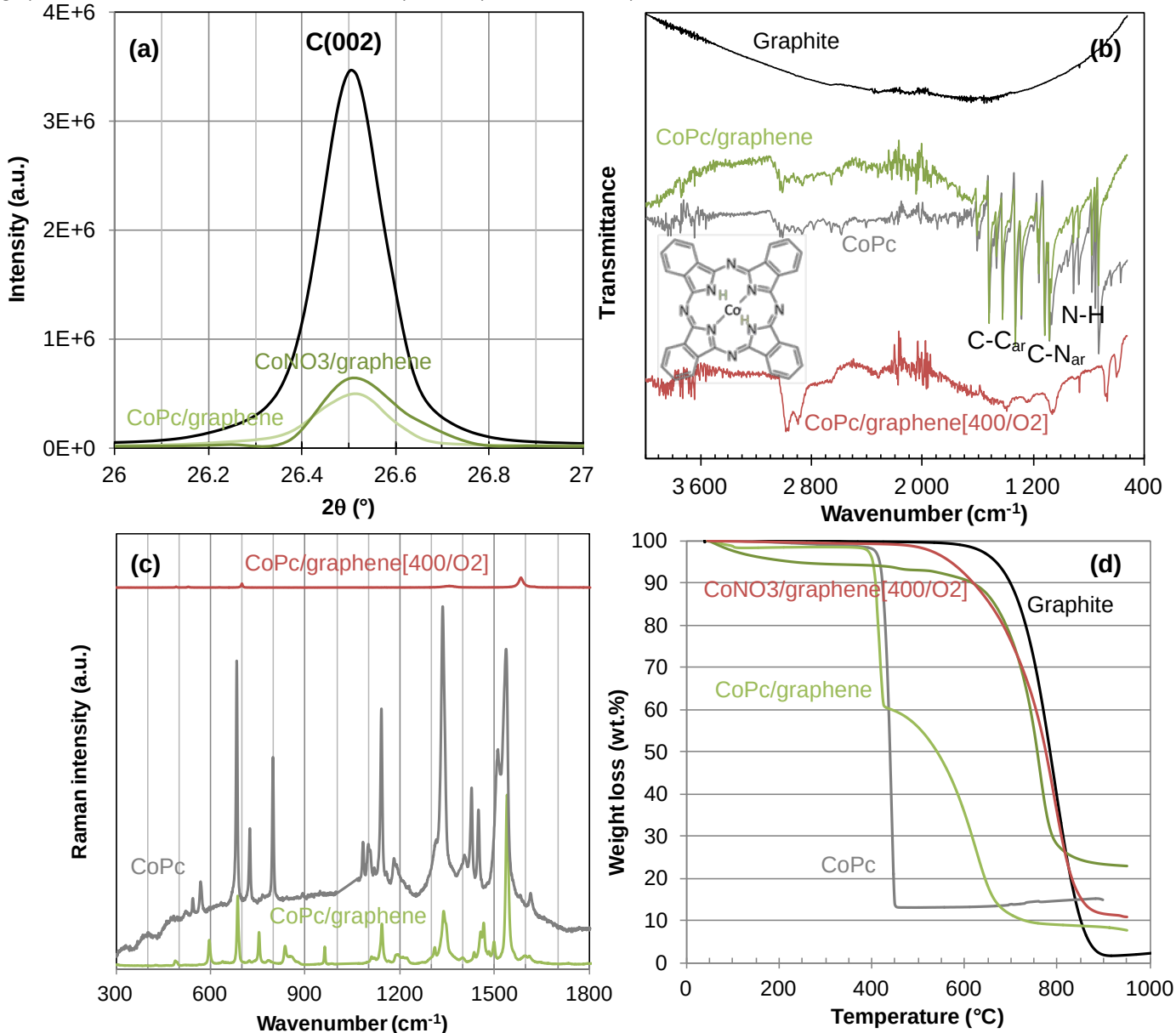

Figure 1. (a) Mass-normalized XRD spectra of graphite (black line), CoPc/graphene (light green line) and CoNO3/graphene(unwashed) (dark green line). (b) FTIR spectra of graphite (black line), CoPc (grey line), CoPc/graphene (green line) and CoPc/graphene[400/O2] (red line). (c) Raman spectra of CoPc (grey line), CoPc/graphene (green line) and CoPc/graphene[400/O2] (red line). (d) TGA of graphite (black line), CoPc (grey line), CoPc/graphene (light green line), CoNO3/graphene (dark green line) and CoNO3/graphene[400/O2] (red line).

This is a clear indication of the pi interaction between CoPc and the graphene surface in the complex, which significantly inhibits the out-of-plane NH vibration of the free complex, leaving the core vibrations unmodified. π interaction between the CoPc complex and the graphene is further supported by TGA studies (Figure 1 d). The thermogravimetric profile of the composite indeed exhibits 2 distinct and sharp weight losses at about 400°C and 430°C, accounting for 40% and ca. 50% of the composite weight. The first one is attributed to the oxidative degradation of Pc, as it matches both the degradation temperature of Pc in the free CoPc complex (Figure 1 d) and the estimated Pc content of the composite based on ICP results (47 wt.%). The second one is attributed to oxidation of the graphitic matrix, which occurs at much lower temperature (~200°C) than the oxidation of the parent graphite. The residual weight (ca. 8%) at 950°C matches well with the presence of the fully oxidized form of cobalt CoO_2 as only residue of the oxidized composite, considering the Co content of the original composite determined by ICP-OES (5.45 wt.%). The virtually unchanged stability of CoPc associated with the drastic decrease in the oxidative stability of graphite in the composite, more specifically the small temperature difference between degradations of CoPc and graphite in the composite, suggests that the oxidation of the graphitic matrix in the composite is triggered by the degradation of CoPc. Hence CoPc and graphene must interact strongly. This is consistent with a strong pi interaction between the extend pi network of graphene and the highly delocalized electrons of the large aromatic Pc ligand. It evidences the presence of 2D CoPc/graphene stacks. The narrow temperature window between the oxidation of Pc and the oxidation of graphite (to CO_2) in the 2D composite has prompted us to investigate calcination treatments with limited amount of oxygen and limited amount of time to yield cobalt oxides from CoPc, while avoiding degradation of the graphitic matrix. A treatment in a flowing (100 mL/min) gas mixture consisting of 10%O_2 in Helium at 400°C for 30 min has finally allowed us to get 3D Co_3O_4/graphene composites, as confirmed by FTIR (Co-O vibrations at 580 and 670 cm^{-1}, Figure 1 b)[20] and XRD (Co_3O_4 (311) and (400) reflections at 2θ = 36.9° and 44.8°, respectively, ICCD No 42-1467, Figure 2 a). Using the Debye-Scherrer equation, an average crystallite size of 25 nm was found for Co_3O_4, based on the full width at half maximum (FWHM) of the (311) reflection. A subsequent treatment under hydrogen using similar conditions (100 mL/min, 400°C, 30 min) yields cobalt metal (33 nm), as shown by the disappearance of Co_3O_4-related XRD reflections and the appearance of a reflection at 2θ = 44.2°, corresponding to (111) of fcc Co (ICCD No 89-4307) (Figure 2 a). It is interesting that all treatments investigated so far to produce CoO_x/graphene from the 2D, pi-stacked CoPc/graphene precursor lead to 3D cobalt oxide nanostructures with little interaction with graphene, as seen in SEM images (Figure 3 b) and further discussed in the TPR section below.

CoNO3-derived composites. For CoNO3/graphene, the FTIR spectrum exhibits a broad 2 peak feature with maxima at 1050 and 1340 cm^{-1} (Figure 2 b). They are attributed to asymmetric stretching vibrations of B-O bonds found in borate compounds ($\nu_{B(4)-O}$ and $\nu_{B(3)-O}$, respectively).[21] Large amounts of sodium and boron are indeed found in CoNO3/graphene, 2.62 and 2.98 wt.% respectively from ICP-OES measurements, in addition to the 7.5 wt.% Co. Besides, sodium metaborate ($NaBO_2.xH_2O$, x=2) is a known product of sodium borohydride oxidation/hydrolysis.[22,23] It may evolve into other complex forms of borates upon exposure to air.[24]

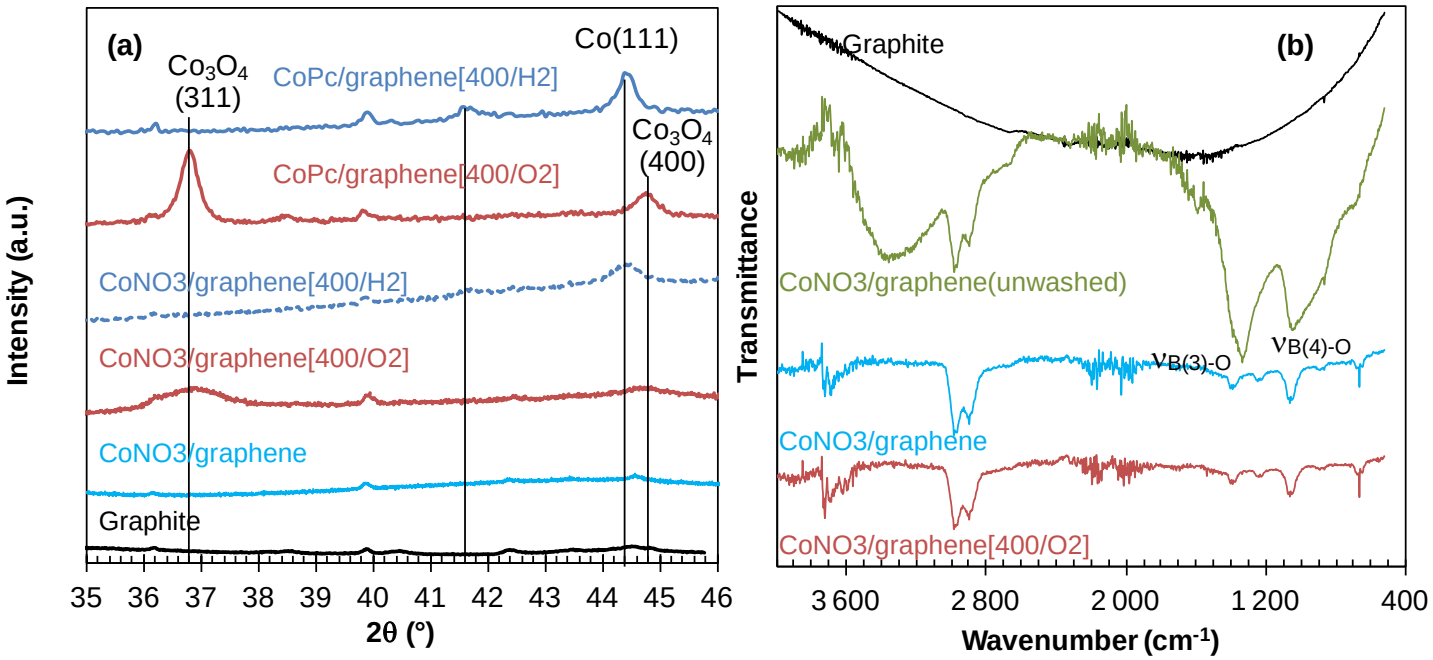

Figure 2. (a) Mass-normalized XRD spectra of (from bottom to top) graphite (black line), CoNO3/graphene (light blue line), CoNO3/graphene[400/O2] (red line), CoNO3/graphene[400/H2] (dotted dark blue line), CoPc/graphene[400/O2] (red line) and CoPc/graphene[400/H2] (dark blue line). (b) FTIR spectra of (from top to bottom) graphite (black line), unwashed CoNO3/graphene (dark green line), CoNO3/graphene (light blue line), CoNO3/graphene[400/O2] (red line).

Presence of such compounds in the unwashed composite is supported by the thermogravimetric profile of the composite (Figure 1 d), which is characterized by a gradual weight loss ranging from 25°C to 500C° in addition to the sharper weight loss at about 600°C corresponding to oxidation of the graphitic component. The first loss, which represents about 10% of the composite weight, is indeed consistent with dehydration and dehydroxylation events of borates, such as e.g. borax.[25] The residual weight (22%), which largely exceeds the weight of the expected CoO_2 residue (11.6%), is also consistent with the presence of a significant amount of borax ($Na_2B_4O_7$). The difference between the borax stoichiometry (Na/B = 0.5) and the actual Na/B molar ratio of 0.4 measured by ICP-OES suggests the presence of other boron-containing compounds, such as e.g. $CoBO_3$. Nevertheless, the application of a straightforward water wash allows the efficient removal of such borates, as evidenced by the disappearance of the two large bands in the FTIR spectrum of the washed composite (Figure 2 b) and the low Na and B contents measured in the washed composite by ICP-OES (<0.03 wt% and <0.08 wt% respectively). The washed composite contains 7.63 wt% of cobalt, but no Co-O vibrations and no Co-related diffraction lines can be observed in the FTIR spectrum (Figure 2 b) and in the XRD spectrum (Figure 2 a) of the washed composites, respectively, despite the prolonged acquisition time used for XRD measurements (see Experimental Section).

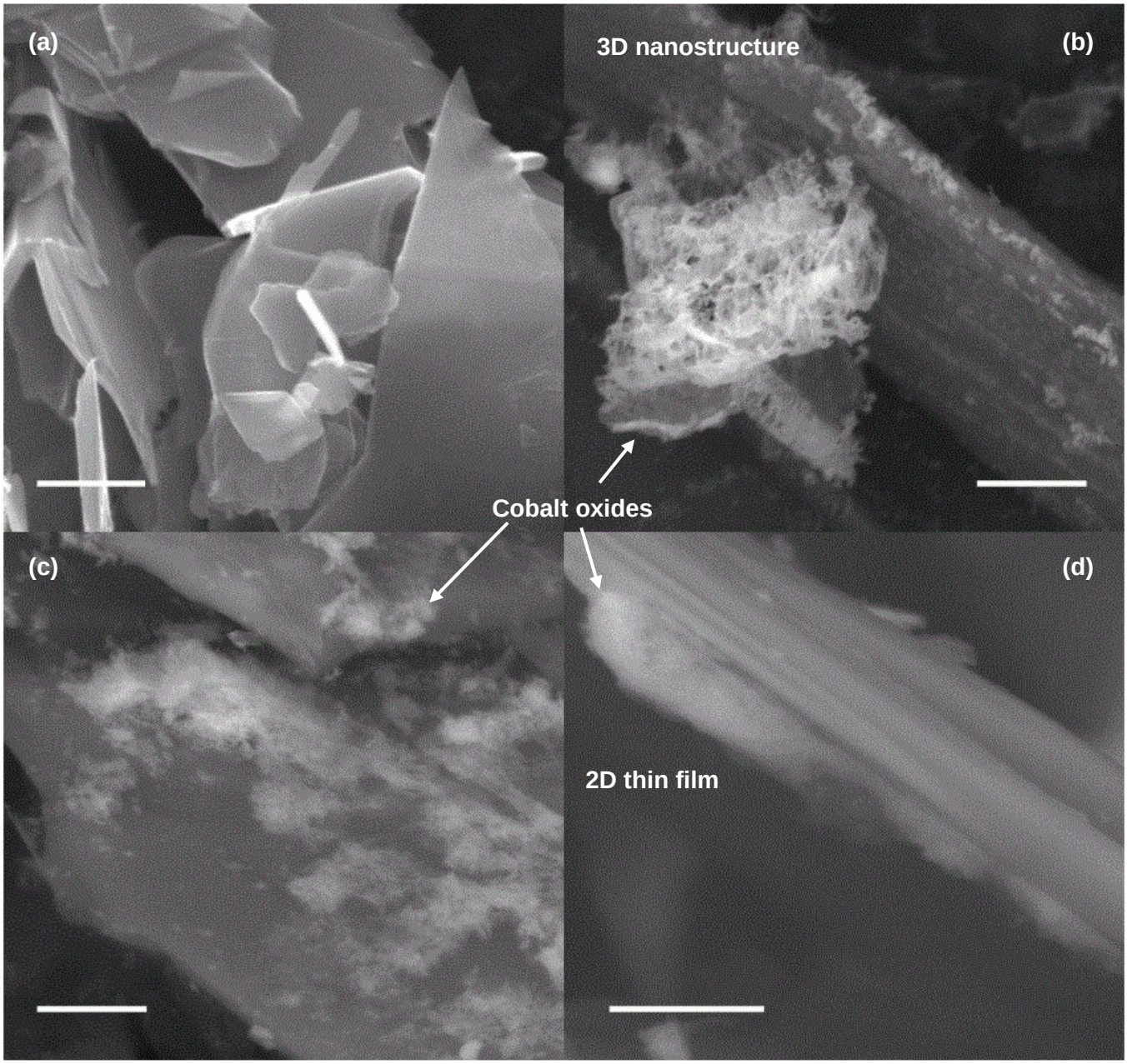

Figure 3. SEM images of the unmodified parent graphite (a), CoPc/graphene[400/O2] (b), CoNO3/graphene (c) and CoNO3/graphene[400/O2] (d). Detector used is BSD for all, except for the parent graphite (In Lens). Cobalt oxides appear in white. Scale bar is 2 μm.

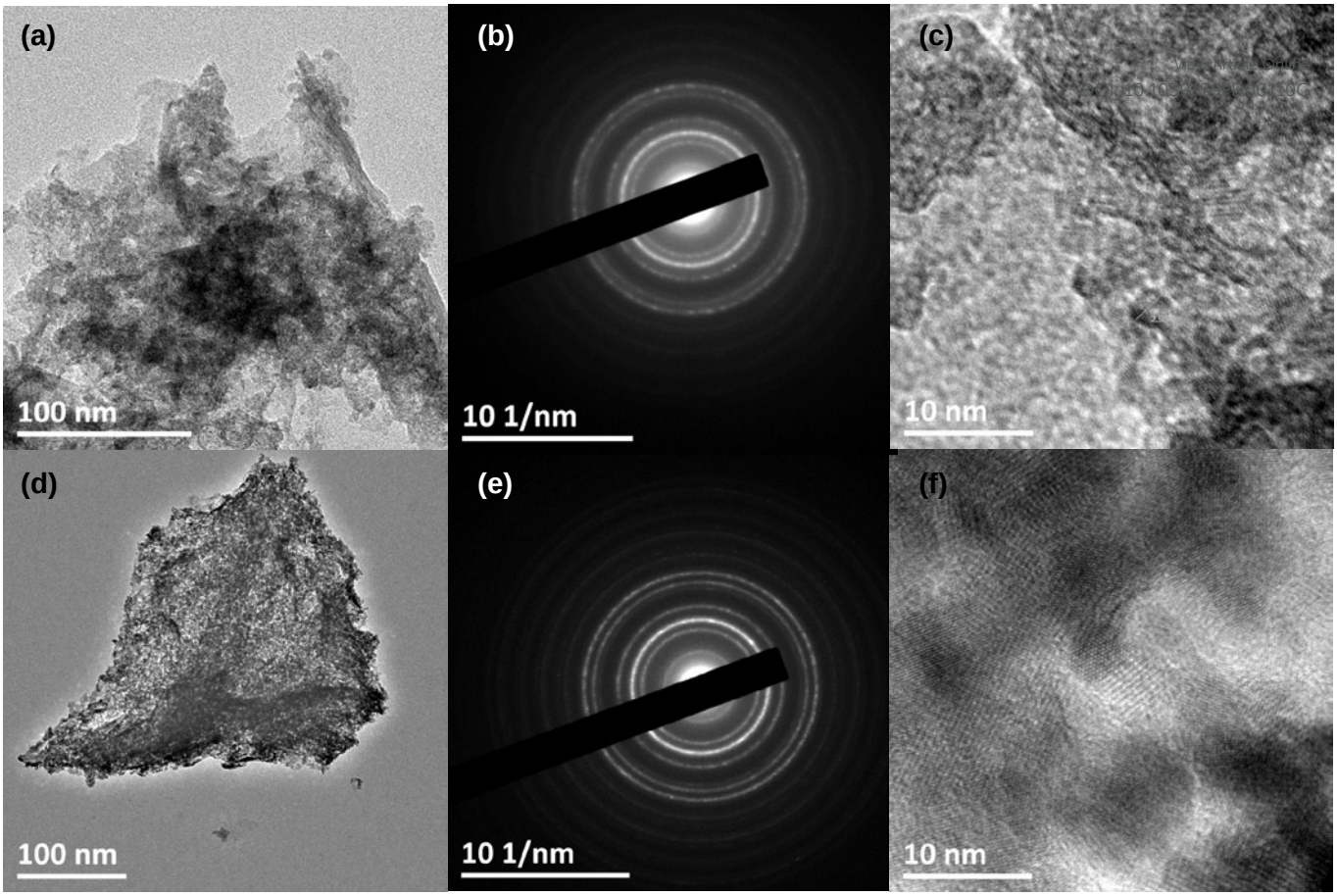

Figure 4. TEM images (a, d), electron diffraction patterns (b, e) and HRTEM images (c, f) of CoNO3/graphene (a-c) and CoNO3/graphene[400/O2] (d-f).

Application of the same calcination treatment as the one used for the formation of supported cobalt oxides from CoPc/graphene (10%O_2/He, 100 mL/min, 400°C, 30 min) results in the appearance of a broad diffraction line at $2\theta = 36.9°$, which can be attributed to the (311) reflection of Co_3O_4 (ICCD No 42-1467) (Figure 2 a). Its full width at half-maximum gives an average crystallite size of 8 nm, which is much smaller than the oxide crystallite obtained in the CoPc route (25 nm). This suggests the presence of a specific morphology for the nitrate-derived oxides. These indeed appear as 2D thin films/patches on SEM images (Figure 3 c, d). They have been further characterized, as detailed below.

Characterization of graphene-supported cobalt oxides from the nitrate route.

Morphology and crystallinity. TEM images of uncalcined CoNO3/graphene clearly show the presence of irregular inorganic, poorly crystallized sheets randomly oriented and dispersed over graphene layers (Figure 4 a). EDX analysis (not shown) shows the presence of cobalt and oxygen. Although no tomography was performed on this sample, the very weak contrast between the Co-containing sheets and the graphene layers suggests that these cobalt oxides sheets are pretty thin (probably less than a few nm thick). The crystallization degree of these sheets is pretty low, considering the very diffuse electron diffraction pattern obtained (Figure 4 b. Nevertheless, very small crystallites of less than 3 nm may be detected by performing HRTEM in the dark field mode (not shown). These nanocrystalline 2D cobalt oxide sheets are consistent with the absence of peak in the X-ray diffraction pattern. TEM images of the calcined sample (Figure 4 d) show a more homogeneous coverage of graphene flakes, suggesting that the randomly distributed cobalt oxide nanosheets have aggregated, and potentially reoriented themselves in a direction more parallel to the graphene layers upon oxidation, to form a more compact 2D film. It is consistent with SEM observations, which show the presence of a more continuous, 1 μm thick film in the calcined composite (Figure 3 d) instead of the smaller and thinner patches of cobalt oxides observed in the uncalcined material (Figure 3 c). The presence of cobalt oxide thin films will be further confirmed by the nitrogen physisorption isotherms presented below. The electron diffraction pattern of these films remains diffuse but it is slightly more pronounced (Figure 4 e). 5-10 nm nanoparticles can be distinguished even in bright field mode. HRTEM shows crystallization domains of about 8 to 10 nm (Figure 4 f), in agreement with the crystallite size derived from the XRD pattern. The larger crystallization domains are likely allowed by reorientation of the 2D sheets and extended crystallization potential in the direction of the graphene planes. d spacings of 0.24, 0.28 and 0.46 nm can be found on bright field images of both

samples. They can be attributed to (311), (220) and (111) interplanar distances of cubic Co_3O_4 (ICCD No 42-1467).[26, 27] d spacings of 0.28 nm and 0.24 may also be attributed to (100) interplanar distances of hexagonal CoO[28] and (111) interplanar distances of cubic CoO.[29] Finally, d spacing of 0.20 nm, corresponding to hcp Co,[28] may also be found on lattice-resolved TEM images of the uncalcined sample (Figure 4 c). Hence, although it is difficult to clearly identify the crystalline composition of cobalt oxides derived from the nitrate route on such low crystallization degree, high resolution bright field images unequivocally show that the extent of crystallization is more advanced in the calcined sample and that as-synthesized CoNO3/graphene is essentially amorphous (Figure 4 c, f).

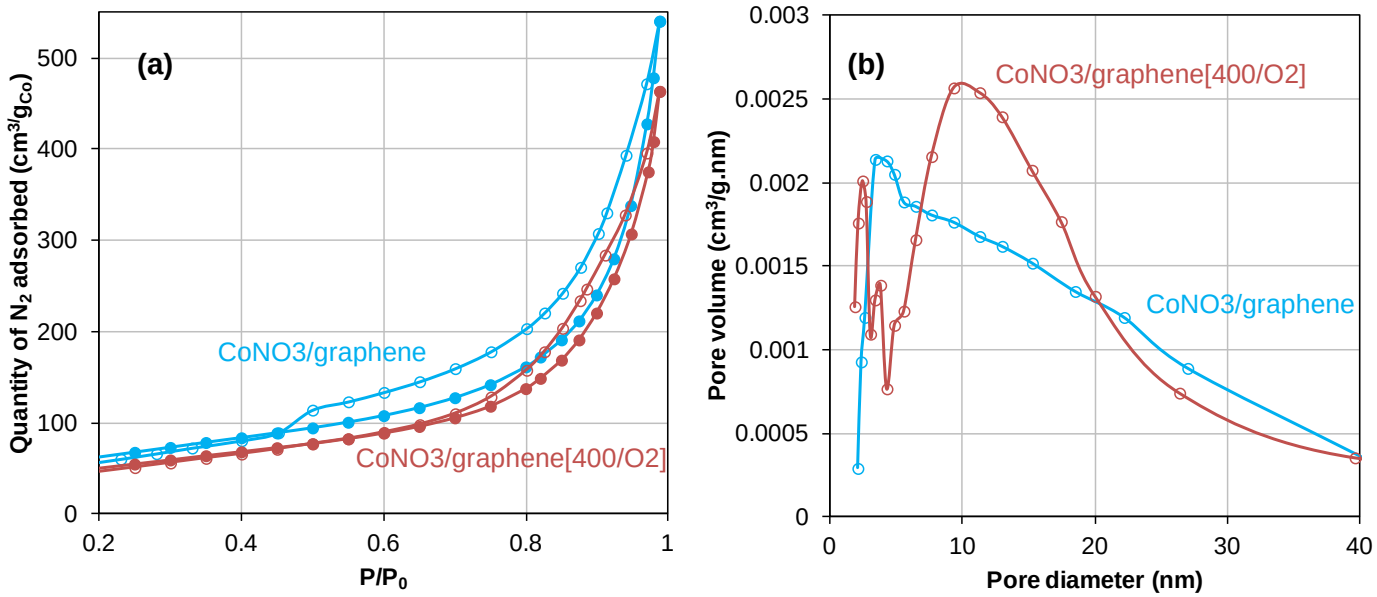

Figure 5. Nitrogen physisorption isotherms (a) and pore size distributions (b) of CoNO3/graphene (light blue line) and CoNO3/graphene[400/O2] (red line),

Porous structuration. N_2 physisorption isotherms and pore size distributions of the CoNO3-derived composites are shown in Figure 5. Both the uncalcined and the calcined materials show Type IV isotherms with H3 hystereses.[30] The specificity of such patterns is that they resemble the reversible Type II isotherms found for non-porous materials, including bulk graphite.[31] Type IV H3 isotherms are generally attributed to loose assemblages of plate-like particles forming slit-like pores. Hence N_2 physisorption isotherms are clearly dominated by the 2D texture of the graphitic component, which represents more than 90% of the total composite mass. Nevertheless, unlike graphite, both composites exhibit significant specific surface area and pore volume. The uncalcined and calcined materials exhibit the same specific surface area of 17.5 (± 0.5) m^2/g and similar overall pore volumes of 0.067 and 0.069 cm^3/g, respectively. However subtle differences may be observed in the isotherm shapes and pore size distributions. The isotherm of the calcined material in particular is very similar in shape to the isotherms of bulk graphitic materials (Type II isotherm). This is consistent with the 2D cobalt oxide films observed on top of graphitic stacks by SEM (Figure 3 d). It suggests that the disordered cobalt oxide sheets of the uncalcined composite have indeed aggregated upon calcination, yet remaining in strong interaction with the graphitic component and thus forming a 2D film parallel to the graphitic structure. The pore size distribution spreads over the 5 to 30 nm diameter range, yet showing a distinct maximum at about 10 nm. It is attributed to the interparticle porosity formed by agglomerated 8 to 10 nm Co_3O_4 crystallites on top of graphene layers. On the other hand, the uncalcined material exhibits a much less defined pore size distribution. It spreads over the 2 to 40 nm diameter range with a much weaker maximum at about 5 nm. It is consistent with the random distribution and orientation of the less dense arrangement of poorly crystallized 2D cobalt oxide sheets on top of graphene layers and the resulting presence of both large intersheet porosity and small intrasheet porosity. Besides, the presence of a small steep at the relative P/P_0 pressure of about 0.5 is a clear indication of the contribution of the porous cobalt oxide component of the composite.[31] In fact, by assuming a negligible contribution of the graphitic matrix (usually < 1 m^2/g and < 0.001 cm^3/g) to the overall surface area of the composites, quite high surface areas can be found for the supported cobalt oxide films of 230 m^2/g_{Co} and 191 m^2/g_{Co} (or 169 m^2/g_{Co3O4} (181 m^2/g_{CoO}) and 137 m^2/g_{Co3O4}) in the uncalcined and calcined composites, respectively. These values are of the same orders of magnitude as those obtained by sophisticated plasma treatment[26] or multi-step templating procedures.[27] Similarly, significant pore volume may be calculated for the cobalt oxide films of 0.64 (0.69 cm^3/g_{CoO}) and 0.55 cm^3/g_{Co3O4} for the uncalcined and calcined films, respectively.

Redox properties of graphene-supported cobalt oxides.

Temperature programmed reduction (TPR) profiles of CoPc/graphene[400/O2], CoNO3/graphene[400/O2] and CoNO3/graphene are shown in Figure 6 a. CoPc/graphene[400/O2]

exhibits the narrowest reduction profile, ranging from 280°C to 500°C. It essentially consists in one peak with a distinct maximum at 400°C. The sharpness of the peak indicates the presence of well-defined, crystalline cobalt oxides.[32] It is consistent with the presence of the large Co_3O_4 crystallites, as determined by XRD. The temperature range also matches that generally observed for the reduction of the Co_3O_4 spinel phase.[32, 33] It is thus attributed to the reduction of Co_3O_4 crystallites. In fact, the narrow profile is very similar to that of unsupported 3D Co_3O_4,[32, 33] suggesting very little interaction of the aggregated Co_3O_4 3D crystallites with the graphene support. It also shows that reduction of Co_3O_4 into Co is thermodynamically completed by 500°C, in complement to the X-ray diffractogram of the reduced CoPc-derived composite showing completion of kinetic reduction to Co in 30 min at 400°C. The reduction profiles of the composites resulting from the nitrate route are much less defined. They range from 200°C to 640°C and from 180°C to 950°C for CoNO3/graphene[400°C/O2] and CoNO3/graphene, respectively. The calcined CoNO3-derived composite exhibits a maxima at 380°C, which is similar to the calcined composite derived from the Pc route, with two shoulders at 330°C and 450°C. The broadness of the reduction peak is consistent with the lower crystallinity of the cobalt oxide component of this sample, as shown by the broad diffraction peak found in the diffractogram. The reduction peak is thus essentially attributed to reduction of the nanocrystalline (8 nm) Co_3O_4 film. The uncalcined CoNO3-derived composite exhibits a yet larger reduction profile with a significantly higher maximum at 500°C and a significantly higher hydrogen consumption. This broad reduction event is consistent with the poor crystallinity of the uncalcined 2D cobalt oxide nanosheets.[32] The shift towards higher reduction temperatures is attributed to the presence of a more reduced phase of cobalt oxide, possibly a CoO-like Co^{2+} cobalt oxide phase.[32]

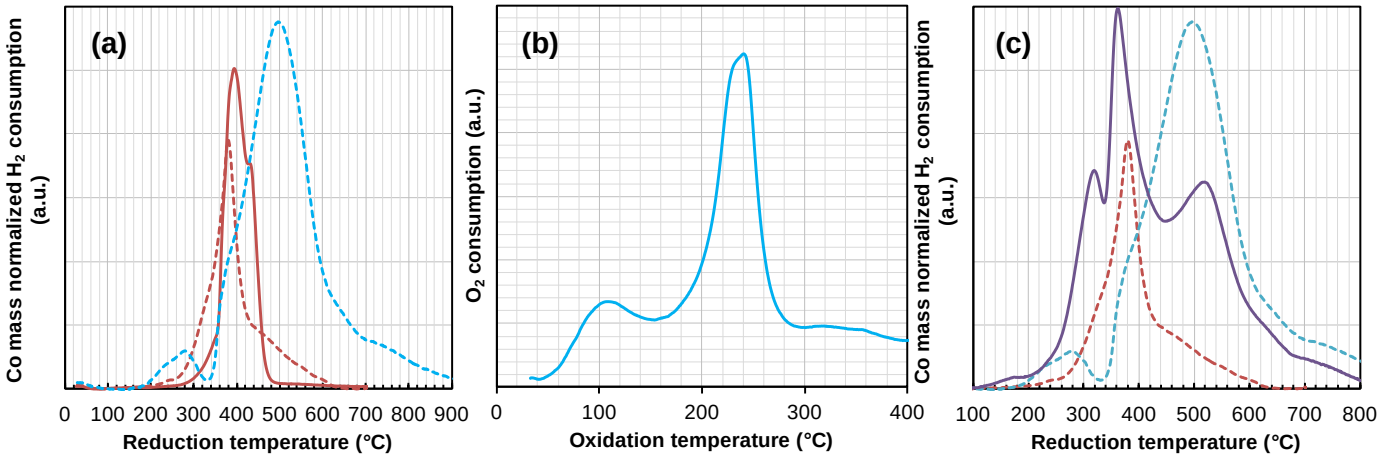

Figure 6. (a) TPR profiles of CoPc/graphene[400/O2] (plain red line), CoNO3/graphene (light blue dotted line) and CoNO3/graphene[400/O2] (red dotted line). (b) TPO profile of CoNO3/graphene. (c) TPR profile of CoNO3/graphene performed after TPO of the sample as compared with CoNO3/graphene before TPO (light blue dotted line) and CoNO3/graphene[400/O2] (red dotted line).

This highly reduced cobalt oxide phase is easily oxidized, as shown by the temperature programmed oxidation (TPO) profile of the material (Figure 6 b). In the TPO, oxidation of the graphene-supported cobalt oxide nanosheets readily starts at 50°C and is completed by 300°C. The pattern exhibits 2 maxima at 110 and 240°C, which could be attributed to the sequential oxidation of Co into CoO and CoO into Co_3O_4.[34] Taking into account the stoichiometry of the reactions ($Co + ½\ O_2 \rightarrow CoO$, $3CoO + ½\ O_2 \rightarrow Co_3O_4$) and the ratio of oxygen consumption of both events (ratio of peak areas ~ 4), relative amounts of Co and CoO present in the uncalcined material may be estimated to be about 20% and 80%, respectively. This is consistent with the shape of TPO profiles and related extent of Co reduction found for other supported cobalt catalysts.[35] However, the low temperature oxygen consumption peak occurs at much lower temperature (ca. -100°C) than usually observed. It is also more clearly defined as usually observed.[36] It could thus more appropriately be attributed to molecular oxygen adsorption[37] on surface oxygen vacancies largely exposed by the 2D configuration of the sheets. Interestingly, a TPR performed after TPO (Figure 6 c) yields a profile similar to that observed over the calcined CoNO3-derived composite (Figure 6 a). The more resolved 3 peak-reduction event, with maxima at 320, 360 and 520°C, is due to the faster temperature ramp used (10°/min instead of than 5°/min) and the lower time held at 400°C (< 1 min vs. 30 min). It is consistent with the predominant presence of Co_3O_4 in a less crystallized state and less compact, less organized 2D film morphology. However, the presence of a small additional hydrogen consumption peak, starting at 100°C with maximum at 170°C, suggests the presence of easily extractable oxygen from the freshly oxidized sample, which could be attributed to adsorbed oxygen. It evidences the very interesting reversible redox properties of the CoNO3-derived composites at low temperature (< 200°C).

Catalytic properties of graphene-supported cobalt oxides for the oxidation of CO.

CO conversions observed in the oxidation of CO as a function of temperature are shown in Figure 7 a. The uncalcined, calcined and reduced CoOx/graphene composites are compared. The uncalcined

CoNO3-derived material yields the lowest temperature of half-CO conversion (T_{50}) of 125°C. The heat-treated CoNO3-derived composites both exhibit T_{50} between 160 and 170°C, regardless of the atmosphere (oxygen or hydrogen) of the heat treatment. The CoPc-derived composites exhibit the highest T_{50} of 190°C, regardless of the atmosphere (oxygen or hydrogen) of the heat treatment. These results show that the initial cobalt phase (Co, CoO or Co_3O_4) present in the composite is less important than crystallinity and morphology of the oxides. Notably, the less crystalline 2D materials (CoO < 3 nm, Co_3O_4 8 nm) are more active for the reaction than the more crystalline phases (Co_3O_4 25 nm, Co 33 nm). It is likely that the poorly crystalline 2D structures contain more oxygen vacancies than the 3D crystals. Besides, the 2D configuration will enhance exposure of oxygen vacancies, hence number of surface oxygen vacancies which have been identified as the active site for the low temperature oxidation of CO.[1, 2] Furthermore, comparison of the less crystalline materials shows that the highly reduced CoO nanosheets are twice as active as the 8 nm Co_3O_4 film (24% and 12% CO conversion observed at 100°C on the uncalcined and calcined CoNO3-derived composite, respectively). The higher surface area of the uncalcined nanosheets (181 m^2/g_{CoO} vs. 137 m^2/g_{Co3O4}) cannot fully account for the superior conversion. Hence the extent of reduction of the cobalt oxide 2D structure appears essential. The superior activity of uncalcined CoO nanosheets is thus attributed to the presence of a highly reduced cobalt oxide phase (Figures 6 a, c) which exhibit unique redox properties below 200°C and, more specifically, which can activate molecular oxygen readily from 50°C (Figure 6 b). The intrinsic activity of these graphene-supported 2D nanosheets is quite high considering the rather low Co content (7.5 wt.%) and low composite mass used in the catalytic evaluation.

The superiority of the uncalcined nitrate-derived composite is also observed in the PROX reaction (CO oxidation in the presence of excess hydrogen, Figure 7 b) and is associated with a high selectivity (> 80% up to 50% O_2 conversion, Figure 7 c). In this reaction, CoNO3/graphene exhibits a T_{50} in the conversion of CO of 205°C. The higher T_{50} as compared to that observed in the absence of hydrogen (125°C) is due to unfavourable competition of CO (1%) with hydrogen (24%) for the limited amount of oxygen (1%) present in the feed.[38] Nevertheless, uncalcined CoNO3/graphene exhibits the lowest T_{50}, and hence the highest activity, as compared with reduced samples (T_{50} of 215°C for both CoNO3/graphene[400°C/H2] and CoPc/graphene[400°C/H2]) and calcined samples (T_{50} of 250°C for both CoNO3/graphene[400°C/O2] and CoPc/graphene[400°C/O2]). In PROX, the nature of the cobalt phase initially present in the composite seems to have more impact than the extent of crystallinity or the 2D vs. 3D morphology. Notably, the more reduced cobalt and cobalt oxides phases are more active than the Co_3O_4 phases, as previously observed.[39] In particular, the graphene-supported CoO-like nanosheets (uncalcined CoNO3/graphene) are now about 10 times more active than the graphene-supported Co3O4 2D film (calcined CoNO3/graphene), showing 28% (vs. 3%) CO conversion at 180°C. The superiority of the 2D nanosheets among the reduced samples can on the other hand be attributed to the higher porosity of the randomly oriented nanosheets and to the more exposed, more numerous oxygen vacancies.

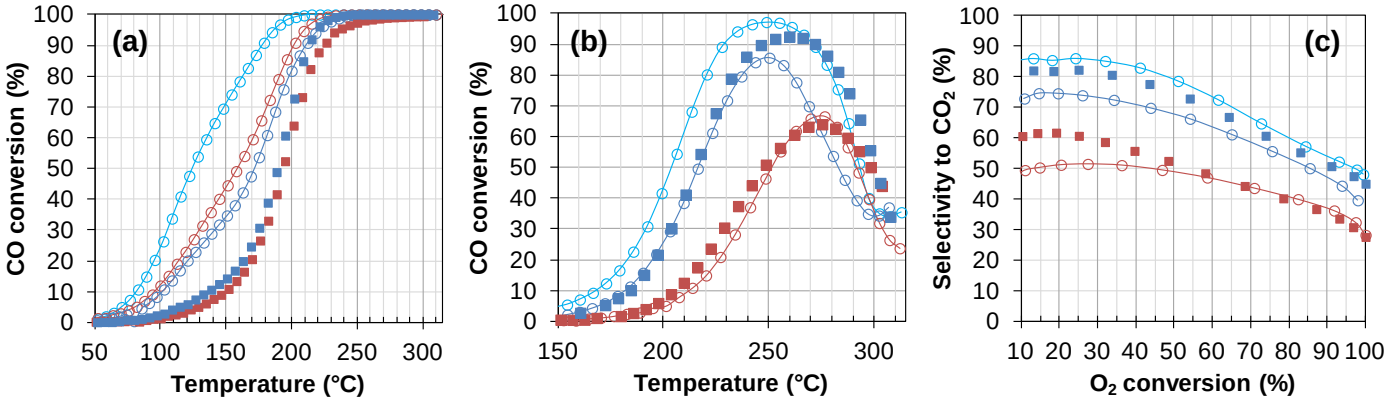

Figure 7. CO conversions observed in the oxidation of CO (a) and in the PROX reaction (b) over CoNO3/graphene (○), CoNO3/graphene[400/O2] (○), CoNO3/graphene[400/H2] (○), CoPc/graphene[400/O2] (□)and CoPc/graphene[400/H2] (□).

Experimental

Materials and syntheses

$Co^{II}(NO_3)_2.6H_2O$ (Puratronic, 99.999% metals basis, Alfa Aesar), Co (II) phthalocyanine (CoPc, Alfa Aesar), N,N-dimethylformamide (DMF, >99.8%, Alfa Aesar), sodium borohydride (≥98%, Sigma Aldrich), graphite powder (natural, high purity 200 mesh, 99.9999 % metal basis, ultra-superior purity, Alfa Aesar) were used without further purification.

High purity graphite (200 ± 2 mg) was dispersed in 200 mL of DMF and sonicated using a Bandelin HD2200 probe sonicator (200 W, 20 kHz), at 50% of its maximum power, during a time t_0 = 5 min. The Co precursor was then added (104 mg for cobalt nitrate and 194 mg for CoPc, 21 mg / 0.36 mmol / 1.8 × 10^{-3} M Co, Co/NG = 0.10 w./w., i.e. Co/(Co+NG) = 9.1% w./w.), after which the mixture was further sonicated for a time t_1 = 5 min. In the case of CoPc, the solid was recovered by hot filtration (final synthesis temperature ~70°C) and dried in air for 16 h at 100 °C. For cobalt nitrate, a given amount of $NaBH_4$ (127 mg / 3.36 mmol / 1.8 × 10^{-2} M, $NaBH_4$/Co = 10) was added before recovery of the solid and the mixture was further

sonicated for a time t_2 = 5 min. Final temperature was about 77±2°C. The solid was then recovered by hot filtration and dried in air for 24 h at 100 °C. After cooling down to 22°C, the sample was washed with deionised water (2*200 mL) and dried in air for 24 h at 100 °C. Two different thermal treatments were applied to the composites: a reducing one in 100%H2 and an oxidative one (calcination) in 10%O_2/He, both under the following conditions: 100 mL/min, 5°/min, 400°C, 30 min. Final composites are denoted *Co precursor*/graphene[*T/atm*], where *Co precursor* stands for the cobalt precursor used (cobalt nitrate or CoPc), *T* and *atm* stands for the final temperature in Celsius and atmosphere of the heat treatment, respectively. Six composites are studied here: CoPc/graphene, CoNO3/graphene, CoNO3/graphene[400/O2], CoNO3/graphene[400/H2], CoPc/graphene[400/O2], CoPc/graphene[400/H2].

Characterization

Elemental analysis (ICP) of the composites was performed by Inductively Coupled Plasma Optical Emission Spectroscopy (ICP-OES, Varian 720ES) at IPHC (CNRS UMR 7178, France) at XXX nm (Co), 249.678 nm (B) and 589.592 nm (Na).

Thermogravimetric analysis (TGA) was performed on TGA Q5000 from TA Instruments. The powder sample (1 mg ± 0.1) was placed in a Pt pan, which was then heated to 1000 °C at 10 °C/min under flowing air (25 mL/min). Evolution of weight loss was monitored by the TA Qseries software.

Temperature programmed reduction and oxidation (TPR/TPO) was carried out on an AutochemII Chemisorption apparatus from Micromeritics equipped with a thermal conductivity detector. The sample (32-50 mg) was loaded in a quartz tube and then heated to:

- 900°C under a flowing mixture of 10%H_2/Ar (10 mL/min) using a temperature ramp of 10°/min for TPR (5 mL/min and 5°/min for CoPc/graphene[400/O2] and CoNO3/graphene[400/O2])

- 400°C under a flowing mixture of 10%O_2/He (10 mL/min) using a temperature ramp of 10°/min for TPO.

Nitrogen physisorption isotherms were obtained on a Micromeritics Asap 2420 porosimeter using N_2 as adsorbent at liquid nitrogen temperature. Materials were outgassed at 150 °C for 4 h prior to analysis. Specific surface areas were obtained via the Brunauer, Emmett and Teller (BET) and t-plot methods.

X-ray diffraction (XRD) patterns of the composites were collected on a Bruker D8 Advance theta-theta diffractometer (Cu Kα radiation, λ = 0.154 nm), equipped with a LynxEye detector and operating at 40 kV and 40 mA. The datasets were acquired in step-scan mode over the 25-58° 2θ range, using a step interval of 0.003° and a counting time of 680.5 s per step. Samples were prepared by weighing out 50 mg of catalyst, using a Eurolabo press at 5 tons, to get flat and smooth pellets, which were then deposited on a round-shaped glass plate. Average CoOx crystalline domains (d_{CoOx}) was determined by the Scherrer equation, using the full width at half-maximum (β = π × FWHM/180) of main CoOx reflections, such as Co_3O_4 (311) at 2θ = 36.9° and Co (111) at 2θ = 44.2°.

$d_{CoOx} = (0.9\ \lambda)/((\beta \times \cos\theta)$

Slight differences in peak positions were observed (e.g. 26.5 ± 0.2° for C(002)). They were attributed to slight differences in the z and corrected by adjusting the position of the C(002) peak maximum at 26.5°.

View Article Online
DOI: 10.1039/C9FD00110G

Fourier transform infrared (FT-IR) spectra were recorded with a Thermo Fisher Nicolet iS10 spectrometer in the 525 – 4000 cm^{-1} range directly on powders (few mg).

Raman spectroscopy was performed on a Horiba Scientific Labram Aramis Raman Spectrometer (Jobin Yvon technology), using a laser wavelength of 532 nm, incident power of 0.4 mW (1 % of the total 40 mW power by applying a D2 filter) and spot size of ~0.8 μm (*100LW lens on Olympus BX41 microscope), hole 200 μm, slit 100 μm, grid 1800. Spectra were recorded in the 100-1000 cm^{-1} and 1065–1805 cm^{-1} regions, with two acquisitions and acquisition time of 150 s for each region. Analyses were performed both in single-spot mode and in dual scan mode (areas of 20 x 20 μm or 30 x 30 μm). Samples were prepared as described for XRD analysis by weighing out 50 mg of material and using an Eurolabo press at 5 tons, to get flat and smooth pellets.

Transmission Electron Microscopy (TEM) was carried out on a JEOL 2100F microscope working at 200 kV accelerating voltage and equipped with a probe corrector for spherical aberrations, giving a point-to-point resolution of 0.18 nm. The sample is dispersed by ultrasound in a chloroform solution for 2 min. A drop of the solution is subsequently deposited on copper covered with a holey carbon membrane and left to dry at ambient temperature (22°C) before observation.

Scanning Electron Microscopy (SEM) was carried out on a Zeiss Gemini SEM 500 system at 12 kV using a working distance (WD) of 11.8 mm and an aperture (AP) of 60 μm. Two detectors were used alternatively: an in lense secondary electron detector (In Lens) for best imaging resolution and a back-scattered electron detector (BSD) providing chemical contrast, with the lightest elements (C) appearing darker than the heaviest elements (Co). An EDXS SDD probe (30 mm^2) confirmed that C, Co and O were the only elements present in the purified materials and that the white spots were indeed cobalt oxides. The powder samples were pressed on a sample holder decorated with carbon tape before analysis.

Catalytic evaluation

Catalytic tests were performed in a fully automated (CETRIB SARL, Andlau, France) fixed-bed flow reactor (i.d. 10 mm) loaded with 26 mg of composite (1.9 – 2.6 mg Co / 32-44 μmol Co). The gas mixtures balanced in He, i.e. 1% CO / 1% O_2 for CO oxidation and 1% CO / 1% O_2 / 24% H_2 for the oxidation of CO in the presence of H_2 (PROX), were introduced at a total flow rate of 100 mL/min (1 atm, GHSV ~ 15,000 h^{-1}). The composite was heated at 1° /min from 20 to 300 °C and then cooled down at the same rate. O_2 and CO conversions were determined on the basis of on-line Compact Gas Chromatograph (Interscience, Belgium) analysis, using external calibration. Selectivity to H_2 is defined as the ratio between the number of mole of O_2 used to convert H_2 (i.e. the total number of mole of O_2 converted minus the number of mole of O_2 used to convert CO) over the total number of mole of O_2 converted.

Conclusions

In conclusion, graphene-supported 2D cobalt oxides can be straight-forwardly synthesized *via* a bottom-up chemical method, by performing $NaBH_4$ reduction of cobalt nitrate during the sonication-assisted exfoliation of graphite in DMF. The highly porous, disorganized, randomly oriented 2D nanosheets of a highly reduced CoO-like phase of cobalt are significantly more active for low temperature CO oxidation than 3D Co_3O_4 nanocrystallites derived from mild oxidation of 2D CoPc/graphene stacks. Their superior activity is attributed to their large porosity and their peculiar low temperature redox properties which suggest the presence of a large number of exposed oxygen vacancies. This study more generally suggests a yet unforeseen role for borax and related borate phases as *in situ* formed hard templates and green structure-directing agents, which can easily be washed off with water, generating unique 2D morphologies and tunable porosities.

Conflicts of interest

There are no conflicts to declare.

Acknowledgements

This work was funded by the French National Research Agency (ANR, PICATA project, ANR-14-OHRI-0005-01). C. Mélard and S. Gallet (University of Strasbourg, CNRS UMR 7515) are thanked for technical support with TGA and Raman studies. F. Vigneron is thanked for technical support with the sonochemical and catalytic reactors. D. Ihiawakrim (IPCMS, CNRS UMR 7504) is thanked for acquiring TEM images. A. Boos, P. Ronot and (IPHC, CNRS UMR 7178) are thanked for performing chemical analyses.

Note after first publication

Figure 2 has been replaced as two of the FTIR spectra were not scaled correctly.

Notes and references

1 Y. Yu, T. Takei, H. Ohashi, H. He, X. Zhang and M. Haruta, *J. Catal.*, 2009, **267**, 121.
2 X. Xie, Y. Li, Z.-Q. Liu, M. Haruta and W. Shen, *Nature*, 2009, **458**, 746.
3 H. Zhang and R. Lv, *J. Materiomics*, 2018, **4**, 95.
4 H. Wang, X. Zhang and Y. Xie, *Mater. Sci. Eng.*, 2018, **R 130**, 1.
5 Y. Liu and X. Peng, *Appl. Mater. Today*, 2017, **8**, 104; Y. Dou, L. Zhang, X. Xu, Z. Sun, T. Liao and S. X. Dou, *Chem. Soc. Rev.*, 2017, **46**, 7338.
6 Y. Zhao, G. I. N. Waterhouse, G. Chen, X. Xiong, L.-Z. Wu, C.-H. Tung and T. Zhang, *Chem. Soc. Rev.*, 2019, **48**, 1972.
7 Y. Sun, S. Gao, F. Lei, C. Xiao and Y. Xie, *Acc. Chem. Res.*, 2015, **48**, 3.
8 T. Zhai, L. Wan, S. Sun, C. Qi, S. Jiao, Q. Xia and X. Hui, *Adv. Mater.*, 2017, **29**, 1604167.
9 Y Cai, J. Xu, Y. Guo and J. Liu, *ACS Catal.*, 2019, **9**, 2558.
10 X. Zhu, H. Ji, J. Yi, J. Yang, X. She, P. Ding, L. Li, J. Deng, J. Qian, H. Xu and H. Li, *Ind. Eng. Chem. Res.*, 2018, **57**, 17394.
11 G.-R. Li, C.-C. Xie, Z.-R. Shen, Z. Chang and X.-H. Bu, *Dalton Trans.*, 2016, **45**, 7866.
12 R. Wang, J. Q. Qi, Y. W. Sui, Y. Chang, Y. Z. He, F. X. Wei, Q. K. Meng, Z. Sun and Y. L. Zhao, *Mater. Lett.*, 2016, **184**, 181.
13 F. Kerdi, V. Caps and A. Tuel, *Stud. Surf. Sci. Catal.*, 2010, **175**, 221.
14 F. Kerdi, V. Caps and A. Tuel, *Micropor. Mesopor. Mater.*, 2011, **140**, 89.
15 C. Marchal, T. Cottineau, C. Colbeau-Justin, V. Caps and V. Keller, *Adv. En. Mater.*, 2018, **8**, 1702142.
16 J. N. Coleman, *Acc. Chem. Res.*, 2013, **46**, 14.
17 K. Guillois, L. Burel, A. Tuel and V. Caps, *Appl. Catal. A*, 2012, **415-416,** 1.
18 F. Vigneron, A. Piquet, W. Baaziz, P. Ronot, A. Boos, I. Janowska, C. Pham-Huu, C. Petit and V. Caps, *Catal. Today*, 2014, **235**, 90.
19 Y. Si and E.T. Samulski, *Chem. Mater.*, 2008, **20**, 6792.
20 J. Preudhomme and P. Tarte, *Spectrochim. Acta A*, 1971, **27**, 1817.
21 L. Jun, X. Shuping and G. Shiyang, *Spectrochim. Acta*, 1995, **51A**, 519.
22 E. Y. Marrero-Alfonso, J. R. Gray, T. A. Davis and M. A. Matthews, *Int. J. Hydrogen En.*, 2007, **32**, 4723.
23 L. Laversenne, C. Goutaudier, R. Chiriac, C. Sigala and B. Bonnetot, *J. Therm. Anal. Calorim.*, 2008, **94**, 785.
24 N. Stepanov, V. Uvarov, I. Popov and Y. Sasson, *Int. J. Hydrogen En.*, 2008, **33**, 7378.
25 I. Waclawska, *J. Therm. Anal.*, 1995, **43**, 261.
26 L. Xu, Q. Jiang, Z. Xiao, X. Li, J. Huo, S. Wang and L. Dai, *Angew. Chem. Int. Ed.*, 2016, **55**, 5277.
27 Q. Yang, Z. Lu, X. Sun and J. Liu, *Sci. Rep.*, 2013, **3**, 3537.
28 X. Deng, D. Yang, G. Tan, X. Li, J. Zhang, Q. Liu, H. Zhang, N. J. Mellors, D. Xuea and Y. Peng, *Nanoscale*, 2014, **6**, 13710.
29 L. Cao, L. Ma, P. Xiao, Y. Zhang, S. Zhang and S. Yang, *Nanotechnol.*, 2014, **25**, 445704.
30 M. Thommes, K. Kaneko, A. V. Neimark, J. P. Olivier, F. Rodriguez-Reinoso, J. Rouquerol and K. S. W. Sing, *Pure Appl. Chem.*, 2015, **87**, 1051.
31 S. Ahmed, A. Ramli, S. Yusup and M. Farooq, *Chem. Eng. Res. Des.*, 2017, 122, 33.
32 P. Arnoldy and J. A. Moulijn, *J. Catal.*, 1985, **93**, 38.
33 G. Grzybek, K. Ciura, J. Gryboś, P. Indyka, A. Davó-Quiñonero, D. Lozano-Castelló, A. Bueno-Lopez, A. Kotarba and Z. Sojka, *J. Phys. Chem. C*, 2019, **123**, 20221.
34 J.-Y. Luo, M. Meng, Y.-Q. Zha and L.-H. Guo, *J. Phys. Chem. C*, 2008, **112**, 8694.
35 G.S. Sewell, E. van Steen and C.T. O'Connor, *Catal. Lett.*, 1996, **37**, 255.
36 J. Jansson, *J. Catal.*, 2000, **194**, 55.
37 Y.-Z. Wang, Y.-X. Zhao, C.-G. Gao and D.-S. Liu, *Catal. Lett.*, 2008, **125**, 134.
38 M. P. Woods, P. Gawade, B. Tan and U. S. Ozkan, *Appl. Catal. B*, 2010, **97**, 28.
39 L. Lukashuk, K. Föttinger, E. Kolar, C. Rameshan, D. Teschner, M. Hävecker, A. Knop-Gericke, N. Yigit, H. Li, E. McDermott, M. Stöger-Pollach and G. Rupprechter, *J. Catal.*, 2016, **344**, 1.